Superradiant Emission from a Collective Excitation in a Semiconductor

T. Laurent, Y. Todorov, A. Vasanelli, A. Delteil, and C. Sirtori*
Université Paris Diderot, Sorbonne Paris Cité, Laboratoire Matériaux et Phénomènes Quantiques, UMR7162, 75013 Paris, France

I. Sagnes and G. Beaudoin
Laboratoire de Photonique et Nanostructures, CNRS, 91460 Marcoussis, France

(Received 19 February 2015; published 29 October 2015)

We report an anomalous wide broadening of the emission spectra of an electronic excitation confined in a two-dimensional potential. We attribute these results to an extremely fast radiative decay rate associated with superradiant emission from the ensemble of confined electrons. Lifetimes extracted from the spectra are below 100 fs and, thus, 6 orders of magnitude faster than for single particle transitions at similar wavelength. Moreover, the spontaneous emission rate increases with the electronic density, as expected for superradiant emission. The data, all taken at 300 K, are in excellent agreement with our theoretical model, which takes into account dipole-dipole Coulomb interaction between electronic excitations. Our experimental results demonstrate that the interaction with infrared light, which is usually considered a weak perturbation, can be a very efficient relaxation mechanism for collective electronic excitations in solids.

DOI: 10.1103/PhysRevLett.115.187402 PACS numbers: 78.60.Fi, 42.50.Ct, 73.21.Fg, 78.67.De

The spontaneous emission rate Γ_{sp}^0 of an isolated "two-level atom" depends exclusively on the energy separation between the levels [1,2]. However Γ_{sp}^0 is not an intrinsic property of the quantum system, as it can be strongly influenced by the electromagnetic environment [3] and/or by the presence of other emitters in the close vicinity of the excited atoms. Both situations have been theoretically and experimentally studied for many years and are known as, respectively, the *Purcell effect* [4] and the *superradiance* [5,6]. This last phenomenon occurs when a dense collection of two-level emitters oscillates in phase, with a consequent increase of the coupling between the light and the ensemble of emitters [7–12]. In the present Letter, we investigate experimentally the superradiant emission from a low-dimensional collective electronic excitation, the intersubband plasmon [13]. So far, the linewidth broadening of intersubband plasmons has been considered exclusively from a solid state physics perspective, invoking strictly nonradiative phenomena such as electron-electron and impurity scatterings [14–16]. We show that the interaction with photons, usually considered only as a weak probe, becomes the dominant relaxation channel in samples with high electronic concentrations. This results in increased linewidths for plasmons with excitation vectors close to the light line.

One of the manifestations of the superradiance phenomena occurs in a cloud of N_e emitters with identical decay rates Γ_{sp}^0, in which only one atom (but we do not know which one) is excited [17,18]. The collective excited state of the system is then a symmetric quantum superposition of all possible states where an atom is in the excited state $|e\rangle$, while all the others are in the ground state $|g\rangle$:

$$|\psi\rangle = (|egg\ldots\rangle + |geg\ldots\rangle + |gge\ldots\rangle + \cdots)/\sqrt{N_e}. \quad (1)$$

This superposition decays exponentially towards the ground state of the system with a time constant $1/(N_e\Gamma_{sp}^0)$, thus N_e times faster than for a single transition. This case has been illustrated in Fig. 1(a), where all the atoms are contained within a volume smaller than λ^3 (λ is the transition wavelength) and it is assumed that atom-atom interactions are absent. Under these assumptions, the excitation spectrum of the N_e atoms is a ladder of equidistant energy levels [top part of Fig. 1(a)], with the first excited state of the ladder precisely of the form $|\psi\rangle$.

In the present work we illustrate that such a superradiance concept can successfully describe the radiative decay in a dense two-dimensional electron gas. This case corresponds to a highly doped quantum well, where the electronic transitions at an energy E_{12} occur between two confined subbands [Fig. 1(b)]. Indeed, in both cases, depicted in panels 1(a) and 1(b), we are dealing with a collection of identical two-level transitions. Apart from obvious considerations on density issues between condensed matter and atomic physics, there are two apparent differences between these systems. The first is that in the atomic configuration the two-level systems are labeled by their position vectors $\vec{r}$ [Fig. 1(a), lower panel], while, for electrons in quantum wells, by the in plane momentum $\vec{k}_{\parallel}$ [Figs. 1(b) and 1(c), middle panel]. The second is that the atomic dipoles are randomly oriented, whereas the optical polarization of the electrons is oriented only in the direction of the confinement. These two considerations and the high electron density are at the origin of a very strong Coulomb

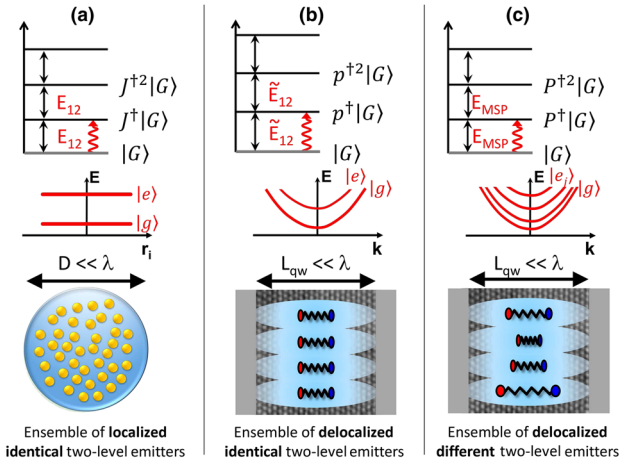

FIG. 1 (color online). Comparison between an atomic ensemble and a two-dimensional electronic system. (a) Different atoms are labeled by their position in the real space and have flat dispersion in the momentum space. Provided that they occupy a volume $\ll \lambda^3$, their spectrum of interaction with the light can be represented as a harmonic ladder. (b) In a two-dimensional electronic system with only two confined subbands there is also a collection of identical two-level emitters, which, however, can be recognized by their momentum in the plane, rather than their positions. Coulomb interaction renormalizes the transition energy by a blueshift, but the overall shape of the optical spectrum stays identical. (c) In the case of several occupied subbands the harmonic spectrum is preserved. Here, the energy spacing E_{MSP} is provided by the many-body interactions, rather than the confining potential. Further explanations are provided in the Supplemental Material [19].

(dipole-dipole) interaction that renormalizes the optical resonance of the system. In the low excitation limit, the many-body excitation spectrum of electrons is also a ladder with an energy spacing $\tilde{E}_{12} = \sqrt{E_{12}^2 + E_p^2}$, with E_p the plasma energy of the electronic ensemble [13,20]. The first collective excitation has a superradiantlike wave function of the form (1) [19,28]. Remarkably, the same harmonic spectrum occurs even for high densities, when electrons occupy different subbands with different energy spacing, as illustrated in Fig. 1(c). In that case the dipole-dipole coupling is so strong that it phases all the oscillators, even at different frequencies, as indicated in Fig. 1(c) [21]. The optical response of the system is then dominated by a single bosonic collective excitation, the multisubband plasmon of energy E_{MSP} which is no longer related to the energy spectrum imposed by the confining potentials [20,21] (Fig. 1(c), top panel). The radiative decay of this many-body plasmon state is inherently superradiant as it is proportional to the number of electrons oscillating in a volume of the order of $\lambda^2 L_{qw}$, that fulfills the Dicke small sample requirement [17].

In this framework the spontaneous emission rate of the multisubband plasmon $\Gamma_{\mathrm{sp}}(\theta)$ can be derived using the Fermi golden rule

$$\Gamma_{\mathrm{sp}}(\theta) = N_s \frac{2\alpha}{m^*} \frac{\pi\hbar}{n} \frac{\sin^2\theta}{\cos\theta} = \beta_s N_s f(\theta), \tag{2}$$

where N_s is the areal electronic density, $\alpha = 1/137$ is the fine structure constant, m^* is the effective mass, n is the refractive index, and θ is the emission angle. On the right-hand side the formula has been further simplified by defining the superradiant coefficient $\beta_s = 2(\alpha/m^*)(\pi\hbar/n)$. The spontaneous emission is thus proportional to the carrier density N_s and it has a strong dependence on the emission angle θ [22–24,29,30], diverging for oblique angles, but it is independent of the energy of the collective excitations. The constant β_s contains the ratio α/m^*, which is reminiscent of elements from quantum optics α and from condensed matter m^*. To clarify the relation between N_s and the total number of electrons participating in the superradiant process N_e it is convenient to express $\Gamma_{\mathrm{sp}}(\theta)$ also as a function of the spontaneous emission rate of a single particle Γ_0:

$$\Gamma_{\mathrm{sp}}(\theta) = N_s \left(\frac{\lambda}{n}\right)^2 \frac{3}{4\pi} \frac{\sin^2\theta}{\cos\theta} \Gamma_0. \tag{3}$$

This expression shows clearly that the number of electrons $N_e = N_s(\lambda/n)^2$ are those contained in an area defined by the wavelength of the emitted photons in the material.

In Fig. 2 the value of the spontaneous emission $\tau_{\mathrm{sp}} = 1/\Gamma_{\mathrm{sp}}$ is plotted as a function of N_s for a collective excitation in a 18.5 nm wide quantum well emitting at $\theta = 60°$ (red line). This is compared with the calculation of the radiative lifetime of a single emitter $\tau = 1/\Gamma_0$ (blue line)

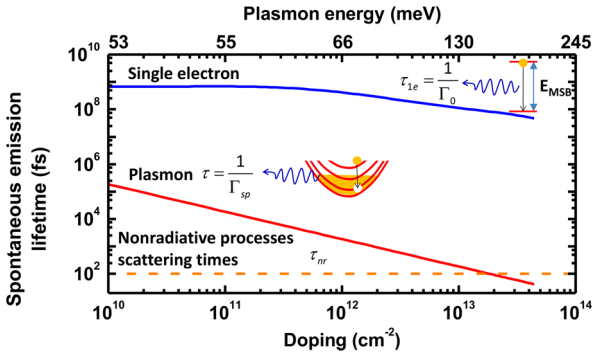

FIG. 2 (color online). Spontaneous emission times as a function of the doping level for superradiant emission from the multisubband plasmon (red line, our case) at $\theta = 60°$ and a single two-level emitter (blue) with the same energy as the collective excitation. The dashed line indicates the typical nonradiative lifetime in intersubband systems. With our doping level ($\approx 10^{13}$ cm^{-2}), the collective excitation has an emission lifetime that is 6 orders of magnitude shorter than that of a single emitter. Furthermore, the radiation lifetime becomes comparable with the nonradiative lifetime, a situation that is unprecedented for a solid state system at room temperature.

that has the same energy as the collective excitation ($E_{12} = E_{\mathrm{MSP}}$). Note that for the values of doping used in our samples ($\approx 10^{13}$ cm^{-2}) the superradiant enhancement gives a spontaneous emission time approximately 6 orders of magnitude faster than for a single emitting dipole. Moreover, in this limit the radiative broadening is expected to be larger than the typical values of the intrinsic broadening due to nonradiative processes.

In order to measure the superradiant emission rate from a high density electron gas, as suggested by Eq. (2), we have studied the emission from samples with different areal doping N_s, as a function of the angle θ. We have analyzed three single quantum well samples, grown by metal organic chemical vapour deposition, that consist of an InGaAs heavily doped layer sandwiched between two AlInAs barriers. The quantum well widths are 18.5 nm for two samples and 100 nm for the third. The surface densities N_s are 1.5×10^{13} cm^{-2} and 2.2×10^{13} cm^{-2} for the wells with identical widths, and 8×10^{13} cm^{-2} for the large well.

The emission from the plasmon resonance is obtained by heating of the electrons in the quantum well, in analogy to previous studies with parabolic quantum wells [31,32]. For this purpose, the samples are processed into field effect transistorlike structures [inset Fig. 3(a)], consisting of two Ohmic contacts (Ni/Ge/Au/Ni/Au annealed at 400 °C) for source and drain (SD), and a nonalloyed Ti/Au layer for the gate [Fig. 3(a)]. The gate size is $L \times W = 50 \times 50$ μm^2, where L and W are, respectively, the length and the width of the channel. In this configuration, due to the very low electronic heat capacity the temperature of the gas can be modulated at high frequency. We can thus detect the

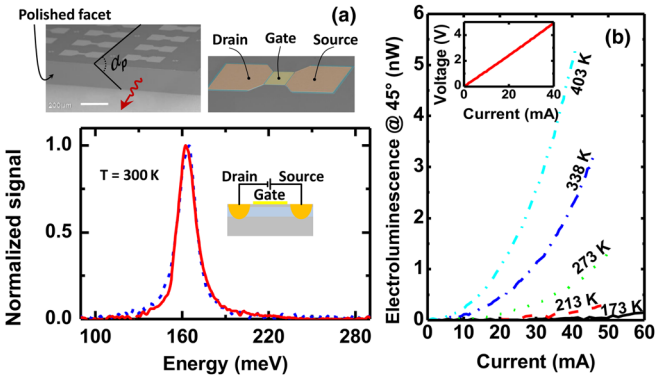

FIG. 3 (color online). (a) Top: SEM images of a facet and a single device (false colors). Bottom: comparison between an absorption spectrum (blue, dashed line) with an emission spectrum (red, continuous line) for a 18.5 nm wide quantum well doped at 2.2×10^{13} cm^{-2}. Both spectra are taken at 300 K and $\theta = 45°$. Inset: a device cross-section illustrating the source (S) to drain (D) bias scheme. (b) Light vs current (L-I) characteristics for an emission angle $\theta = 45°$ and different heat sink temperatures. Notice that the 173 K curve is barely visible above the noise level. Inset: V-I characteristic of the same device at 338 K.

plasmon emission with a lock-in technique which eliminates the black-body radiation background of the substrate. Samples are mounted either in a cryostat or on a heating device that allows changing the substrate temperature from 4 to 400 K, which permits us to vary the heat capacity of the electrons that increases exponentially with temperature. Emission is measured through the polished facet of the semiconductor substrate [Fig. 3(a), top].

In the main part of Fig. 3(a) we present plasmon emission (continuous line) and absorption spectra (dotted line), measured at 300 K, for the sample with 18.5 nm well width and electronic density 2.2×10^{13} cm^{-2}. Both spectra have been measured with an angle $\theta = 45°$ in a Fourier transform infrared spectrometer. The emission spectrum is obtained by injecting 30 mA current. The two spectra overlap remarkably well, meaning that the same excitation is measured in absorption and emission. Both peaks are centered at $E_{\mathrm{MSP}} = 161$ meV and have a full width at half maximum (FWHM) of ≈ 14 meV. Notice that in spite of the disorder that is introduced by the high concentration of donors, at this angle, the measured peaks are quite narrow (FWHM$/E_{\mathrm{MSP}} = 9\%$).

In Fig. 3(b) the electrical and optical characteristics of our device are reported. Light versus current characteristics (L-I) at different heat sink temperatures are shown in the main panel for $\theta = 45°$. In the inset we present the voltage-current (V-I) characteristic at 338 K for the SD injection, while no voltage is applied to the gate in this work. The V-I is perfectly Ohmic. The current, modulated with a squared wave at 10 kHz, is injected by applying a bias across SD to heat the electron gas and increasing the overall temperature of the system. Plasmons are thus thermally promoted on the excited states and relax radiatively. This is confirmed by the quadratic dependence of the luminescence as a function of the injected current. Moreover, the intensity of the signal varies exponentially with the heat sink temperature, as expected from the temperature dependence of the electronic heat capacity.

The main results of our investigation are reported in Fig. 4, where we measure the spectra as a function of the emission angle θ. The experiment is illustrated on the left side of Fig. 4. Emission spectra of our devices are presented on the three-dimensional color plots of Fig. 4, as a function of the photon energy and θ. In order to scan a wide angular range each panel is composed of spectra taken at four different polishing angles α_p (30°, 45°, 60°, 80°). For all samples, the width of the spectra increases at higher angles, due to the rise of the spontaneous emission rate that becomes the dominant contribution in the emission linewidth towards 80°. The broadening increases faster for higher doping as expected from Eq. (2). Close to 90°, however, the linewidth does not follow the dependence and decreases, as it has been already shown for the case of z-polarized exciton-polaritons that have similar angular dependence [24,30]. The increase of the linewidth with the

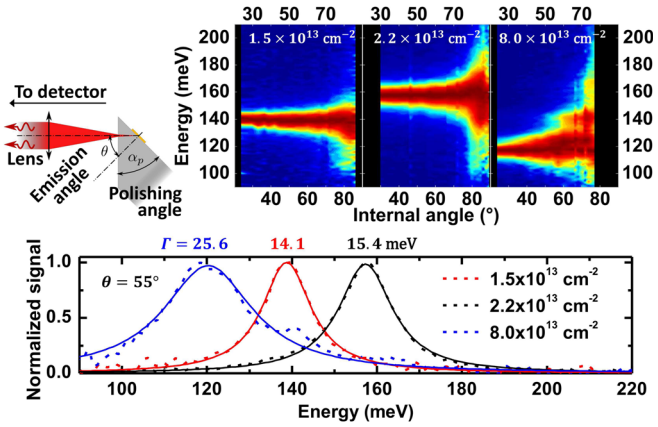

FIG. 4 (color online). Top left: scheme of our experimental configuration for collecting plasmon emission. Top right: color maps of the normalized emission spectra of samples with three different dopings. Bottom panel: the dotted lines are the normalized spectra of the three samples for $\theta = 55°$. The continuous lines indicate Lorentzian fits.

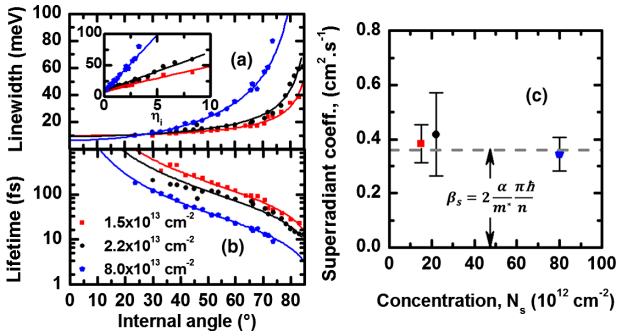

FIG. 5 (color online). (a) Spectral linewidths extracted from the data in Fig. 4 as a function of θ, for the three different doping levels. The inset reports the same curves plotted as a function of $\sin^2\theta/\cos\theta$ and the corresponding linear fits. Their slopes provide directly the rate factor $N_s\beta_s$ from Eq. (2). (b) Radiative lifetimes of plasmons as a function of θ obtained by subtracting the nonradiative contribution. (c) Superradiant coefficient β_s obtained by dividing the slopes of the linear fits in (a) by the doping concentration of the samples N_s. The gray dashed line represents the value $\beta_s = 2(\alpha/m^*)(\pi\hbar/n)$.

sample doping is also clearly evidenced in the lower part of Fig. 4 where we report three representative spectra of the samples taken at $\theta = 55°$. Note that none of the possible nonradiative scattering mechanisms, such as optical phonon, interface roughness, or electron-electron scatterings depends on the angle of the emitted photons, and therefore cannot explain the observed experimental results. Indeed, the investigated photon momenta are always too small on the scale of the Brillouin zone, and cannot induce such strong variations in the nonradiative decay rates.

In Fig. 5(a) we summarize the dependence of the FWHM of the spectra reported in Fig. 4 as a function of θ. Data are very well fitted with the angular dependence of Eq. (2), $\sin^2\theta/\cos\theta$ up to 85°, and assuming a total linewidth $\Gamma_{sp} + \gamma$, with γ the intrinsic nonradiative contribution. This contribution can be recovered from Fig. 5(a) as the limit of the linewidth when $\theta \to 0°$. We obtain $\gamma \approx 10$ meV for the two 18.5 nm quantum well samples and 6.6 meV for the 100 nm one. For angles above 60°–70° the linewidth is dominated by the radiative component Γ_{sp}, a very unusual situation in condensed matter physics at room temperature or above. In the inset, the data of Fig. 5(a) are plotted on a linear scale as a function of $\eta = \sin^2\theta/\cos\theta$. This is done to better separate the dependence on the density, which is now proportional only to the slope. One can clearly see that the samples doped 1.5×10^{13} cm^{-2} and the 2.2×10^{13} cm^{-2} have two well-distinct slopes. In Fig. 5(b) we extract the value of the spontaneous emission lifetime from the data of Fig. 5(a), by subtracting the intrinsic width γ from the total linewidth, and taking the reciprocal of the remaining radiative width. It is remarkable that for all samples the spontaneous emission lifetime reaches tens of femtoseconds at high angles, to compare with a hundred nanoseconds for a single electron. From the three slopes obtained with the linear fits in Fig. 5(a) we can derive the experimental values of the superradiant coefficient for each sample. As shown in Fig. 5(c) this value is constant for all the samples within the experimental error. Note that the calculated value of the superradiant coefficient is $\beta_s = 0.36$ [cm$^2 \cdot$ s^{-1}].

In conclusion, we have predicted and measured superradiant spontaneous emission from a dense ensemble of electrons in a two-dimensional potential well. This physical system fulfils the conditions to observe superradiance, namely small size and high densities. Moreover, dipole-dipole Coulomb coupling for this highly symmetric system favors the appearance of superradiant states. Spontaneous emission shorter than 100 fs has been measured. These results show the existence of radiative lifetime limited excitations in solid state systems at room temperature and above. Finally, this phenomenon hints to new possible mechanisms for efficient light generation and ultrafast sampling of time-based signals. In particular, superradiant states can be used to realize monochromatic incandescent midinfrared sources [33–35], with unprecedented modulation bandwidth.

The authors acknowledge financial support from ERC grant "ADEQUATE" and by the French Renatech Network.

*carlo.sirtori@univ-paris-diderot.fr

[1] C. Cohen-Tannoudji, J. Dupont-Roc, and G. Grynberg, *Photons et Atomes: Introduction à l'Électrodynamique Quantique* (EDP Sciences, Paris, 2001).

[2] G. Grynberg, A. Aspect, and C. Fabre, *Introduction to Quantum Optics: From the Semi-Classical Approach to Quantized Light* (Cambridge University Press, New York, 2010).

[3] R. R. Chance, A. Prock, and R. Silbey, Adv. Chem. Phys. **37**, 1 (2007).
[4] E. M. Purcell, H. C. Torrey, and R. V. Pound, Phys. Rev. **69**, 37 (1946).
[5] R. H. Dicke, Phys. Rev. **93**, 99 (1954).
[6] N. E. Rehler and J. H. Eberly, Phys. Rev. A **3**, 1735 (1971).
[7] N. Skribanowitz, I. P. Herman, J. C. MacGillivray, and M. S. Feld, Phys. Rev. Lett. **30**, 309 (1973).
[8] M. Gross, P. Goy, C. Fabre, S. Haroche, and J. M. Raimond, Phys. Rev. Lett. **43**, 343 (1979).
[9] Y. Kaluzny, P. Goy, M. Gross, J. M. Raimond, and S. Haroche, Phys. Rev. Lett. **51**, 1175 (1983).
[10] R. J. Thompson, G. Rempe, and H. J. Kimble, Phys. Rev. Lett. **68**, 1132 (1992).
[11] Y. O. Dudin, L. Li, F. Bariani, and A. Kuzmich, Nat. Phys. **8**, 790 (2012).
[12] Q. Zhang, T. Arikawa, E. Kato, J. L. Reno, W. Pan, J. D. Watson, M. J. Manfra, M. A. Zudov, M. Tokman, M. Erukhimova, A. Belyanin, and J. Kono, Phys. Rev. Lett. **113**, 047601 (2014).
[13] T. Ando, A. B. Fowler, and F. Stern, Rev. Mod. Phys. **54**, 437 (1982).
[14] J. B. Williams, M. S. Sherwin, K. D. Maranowski, and A. C. Gossard, Phys. Rev. Lett. **87**, 037401 (2001).
[15] C. A. Ullrich and G. Vignale, Phys. Rev. Lett. **87**, 037402 (2001).
[16] C. A. Ullrich and G. Vignale, Phys. Rev. B **65**, 245102 (2002).
[17] M. Gross and S. Haroche, Phys. Rep. **93**, 301 (1982).
[18] M. O. Scully and A. A. Svidzinsky, Science **325**, 1510 (2009).
[19] See Supplemental Material at http://link.aps.org/supplemental/10.1103/PhysRevLett.115.187402, which includes Refs. [1–3,13,17,18,20–27], for theoretical description of the superradiance in highly doped QWs, as well as complementary experimental data.
[20] G. Pegolotti, A. Vasanelli, Y. Todorov, and C. Sirtori, Phys. Rev. B **90**, 035305 (2014).
[21] A. Delteil, A. Vasanelli, Y. Todorov, C. Feuillet Palma, M. Renaudat St-Jean, G. Beaudoin, I. Sagnes, and C. Sirtori, Phys. Rev. Lett. **109**, 246808 (2012).
[22] C. Ciuti and I. Carusotto, Phys. Rev. A **74**, 033811 (2006).
[23] F. Tassone, F. Bassani, and L. Andreani, Nuovo Cimento Soc. Ital. Fis. **12D**, 1673 (1990).
[24] F. Alpeggiani and L. C. Andreani, Phys. Rev. B **90**, 115311 (2014).
[25] T. Holstein and H. Primakoff, Phys. Rev. **58**, 1098 (1940).
[26] Y. Todorov and C. Sirtori, Phys. Rev. B **85**, 045304 (2012).
[27] S. M. Sze, *Physics of Semiconductor Devices* (J. Wiley and Sons, New York, Chichester, Brisbane, 1981).
[28] Y. Todorov and C. Sirtori, Phys. Rev. X **4**, 041031 (2014).
[29] K. Cho, J. Phys. Soc. Jpn. **55**, 4113 (1986).
[30] C. Creatore and A. L. Ivanov, Phys. Rev. B **77**, 075324 (2008).
[31] K. D. Maranowski, A. C. Gossard, K. Unterrainer, and E. Gornik, Appl. Phys. Lett. **69**, 3522 (1996).
[32] J. Ulrich, R. Zobl, K. Unterrainer, G. Strasser, E. Gornik, K. D. Maranowski, and A. C. Gossard, Appl. Phys. Lett. **74**, 3158 (1999).
[33] M. De Zoysa, T. Asano, K. Mochizuki, A. Oskooi, T. Inoue, and S. Noda, Nat. Photonics **6**, 535 (2012).
[34] X. Liu, T. Tyler, T. Starr, A. F. Starr, N. M. Jokerst, and W. J. Padilla, Phys. Rev. Lett. **107**, 045901 (2011).
[35] J.-J. Greffet, Nature (London) **478**, 191 (2011).